Measurement of Ultrathin (<100 Å) Oxide Films by Multiple-Angle Incident Ellipsometry

Tien Sheng Chao, Chung Len Lee, and Tan Fu Lei

Institute of Electronics, National Chiao Tung University, Hsinchu, Taiwan, China

ABSTRACT

The application of the multiple-angle incident ellipsometry to measure the ultrathin (<100 Å) oxide has been studied in this paper. First, four interfacial models are investigated by using a fitting scheme to fit ellipsometric data (Δ, ψ) at various incident angles, and the abrupt model is found to be the most appropriate model to model the transition region of the SiO_2-Si interface. The sensitivities on the incident angle and the errors induced by the ellipsometric parameter variations are also analyzed. Ellipsometry is applied to measure the native oxides of Si wafers after they are treated with different cleaning processes, and it is also applied to measure refractive indexes and thicknesses of ultrathin thermally grown SiO_2. It is believed that these are the most accurately measured results on the refractive indexes of ultrathin oxides. Also, an empirical formula for thermal oxide growth in dry O_2 is obtained.

Thin dielectrics find many applications in metal oxide semiconductor (MOSFET) devices, especially as the gate insulators of MOSFET. As very large scale integrated (VLSI) technology continues to advance, the gate insulators, usually oxides, are getting thinner and thinner. It is predicted that, at the year of 2000, the thickness of the gate oxide will be 40 Å (1). Much research work has been devoted to studying the preparation, physics, and device applications of thin dielectrics (2, 3). In these studies, it is important to measure precisely the thickness of thin dielectric. For example, one of the needs is to measure accurately the thickness of thin oxides in studying their oxidation kinetics, especially at the initial oxidation stage (4-6), in order to accurately model the growth process. Another example is that, in studying the carrier conduction mechanism in tunneling oxides for their applications in the electrically erasable programmable read-only memory (EEPROM), it is required to obtain the exact thickness of oxides in order to properly model the carrier conduction process, since several angstroms of error in the oxide thickness could lead to one order of magnitude deviation in calculating the *I-V* characteristics (7, 8).

To measure the oxide thickness, ellipsometry is usually employed because of its simplicity, nondestructiveness, and easy sample preparation (9). As early as 1957, this method had been used to study the oxide growth kinetics of silicon and germanium when they were exposed to the room air (10). Besides measuring thickness, it can also measure the refractive index of the film. Today, ellipsometers, either the nulling type or the rotary type, have been manufactured as automatic instruments to characterize thin films and the measurement results can be obtained within 30 s for one measurement (9). However, when it is applied to measure ultrathin dielectric films, serious errors could occur due to measurement random errors and the instrumental systematic errors (11, 12). It has been shown (11) that for the Si-SiO_2 system, to measure SiO_2 of the thicknesses less than 200 Å, errors in the obtained thickness and the refractive index could exceed 50%. To reduce these errors, a technique has been proposed by employing a ϕ *vs.* T plot, where ϕ is the incident angle of the light beam of the ellipsometer and T is the thickness of the measured film (12). This technique has been extended to measure the refractive index profile of thin films (13).

To measure the precise thickness of the ultrathin oxide with ellipsometry, a common practice is that the measured ellipsometric data (Δ, ψ) are substituted into ellipsometric equations (11) to solve for the thickness T by assuming a known value for the refractive index N for the oxide. The obtained oxide thickness is then doubly checked with the data obtained with the C-V measurement on the metal oxide capacitor (MOS) capacitor made with the oxide of the same thickness (14). With this practice, if the N value is assumed rightly, errors can be significantly reduced, as indicated by the analyzed results of Ref. (11). However, as has been reported in Ref. (15, 16), different oxidizing conditions result in oxides of different composition densities and interfacial properties, which consequently lead to different values in the refractive index of the oxide. Also, in the C-V measurement of the MOS capacitor, in order to derive the value of the thickness of the sandwiched oxide, the dielectric constant of the thin oxide must be first assumed. As the thickness of the oxide approaches the range of less than 50 Å, the value of the dielectric constant cannot be assumed to be the same as that of the thick oxide. Also in this range, the carrier tunneling phenomenon becomes important during the C-V measurement, and this makes the thickness derived from the C-V curves inaccurate.

The interfacial property of the Si-SiO_2 system affects the measurement data significantly, especially for the ultrathin (<50 Å) region. Much work has done on this topic based on the use of Auger spectroscopy, electron spectroscopy for chemical analysis (ESCA), Rutherford He backscattering spectroscopy, transmission electron microscopy (TEM), x-ray photoelectron spectroscopy, low-energy ion scattering spectroscopy, infrared spectroscopy and the ellipsometery (17-22). Reference (23) summarizes the results of the above studies on the interfacial transition layer of the Si-SiO_2 system. Although the results are controversial, it is fairly safe to say that different oxidation conditions result in a transition layer of different thickness and optical property, and either an abrupt transition layer of two to three atomic layers or a graded transition layer of smaller than 20 Å can be used to model the interfacial transition layer of the Si-SiO_2 system.

For the ellipsometry measurement on ultrathin oxides, the conventional ellipsometry of single wavelength and single incident angle suffers the drawback of inaccuracy mentioned above. Multiple wavelength ellipsometry had been used, and it offered more than two sets of (Δ, ψ) data which could be used to improve the accuracy for the derived values for N and T (24, 25). However, multiple wavelength ellipsometry suffers the problem of dispersiveness of the measured film. Also, it needs the information of the refractive index at various wavelengths for the silicon substrate. Single wavelength multiple incident angle ellipsometry, which does not have the above problem, offers multiple sets of (Δ, ψ) data which can be used to fit the values for the refractive index and the thickness of the measured film. As early as 1964, Crackin and Colson (26) had used it to measure properties of thin films. In multiple angle incident (MAI) ellipsometry, a fitting procedure is usually employed. Ibrahim and Bashara (27) have studied the parameter correlation for the numerical fitting process and found that the initial guesses on parameters were important on the final computed solutions. It was suggested that the refractive index and the thickness of the measured films should be independently estimated.

In this paper, a null-type MAI ellipsometry with a 6328 Å He-Ne laser source is studied for its application to measure the ultrathin (<100 Å) oxide. Four transition layer models

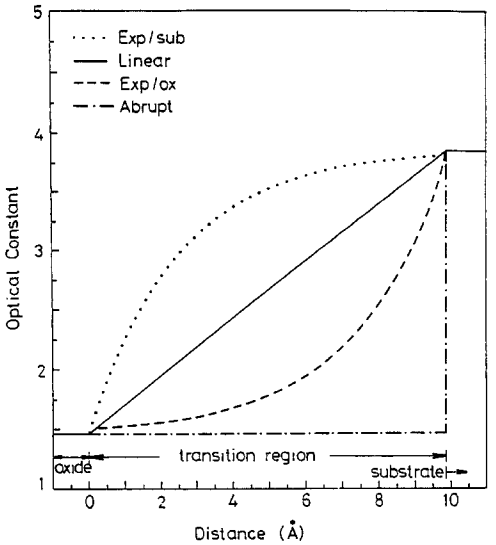

Fig. 1. Four different models for the interfacial transition layer of the SiO_2-Si system. The transition layer is 10 Å thick.

for the SiO_2-Si interfacial layer are first investigated for their use in the MAI ellipsometry. The multiple-angle incident ellipsometry is also studied in terms of the sensitivity in the incident angle and in parameter errors. To demonstrate the powerfulness of this MAI ellipsometry, it is then applied to measure the native oxide of Si wafers in the range of 7-25 Å. It is also applied to measure refractive indexes and thicknesses of the oxides grown at the initial stage of thermal oxidation at different temperatures. It is believed that this is the most accurately measured result on the indexes of ultrathin oxides. An empirical formula for thermal oxide growth in dry O_2 is also obtained.

Transition Layer Models and MAI Ellipsometry

As mentioned previously, the model chosen for the interfacial transition layer affects the calculated values for N and T of the measured film. In this section, four models, namely, the abrupt model, the linear model, the exponential/sub. model and the exponential/ox. model (Fig. 1) for the transition layer (24) are studied by using them to fit the experimental data obtained by the MAI ellipsometry. The fitting errors for each model are then compared in order to identify the most appropriate model for ultrathin oxides in the ellipsometry measurement.

It is assumed that the transition layer is of a thickness of 10 Å and the refractive index of this interfacial transition layer can be expressed by the following equations for the four models, respectively

abrupt model

$$N_{\text{int}} = N$$

linear model

$$N_{\text{int}} = N + (N_{\text{sub}} - N)(x/10)$$

exponential/sub model

$$N_{\text{int}} = N_{\text{sub}} - (N_{\text{sub}} - N)\exp(-4x/10)$$

exponential/ox model

$$N_{\text{int}} = N - (N - N_{\text{sub}})\exp[-4(10 - x)/10]$$

where N_{int}, N, and N_{sub} are the refractive indexes of the interfacial transition layer, the oxide, and the substrate, respectively, and x is the distance in angstroms from the boundary of the oxide to the transition layer. For the MAI ellipsometry, the sample is measured at a set of incident angles and a set of (Δ, ψ) data corresponding to each incident angle are obtained. Figure 2a and b show an example of plots of the measured Δ, ψ (the dotted values) *vs.* the incident angle in the range of 65-72°, respectively, for several experimental samples. The samples were silicon wafers oxidized in dry O_2 at 900°C for 10, 20, 30, and 40 min, respectively. The plots are curve fitted to obtain the values for the thickness and the refractive index, the corresponding fitted values for the thickness, the refractive index, and the sum of least squares error for each model are shown in the Table I. In the table, it can be seen that, as the oxide becomes thinner, the fitting errors for each model increase. This means that as the oxide thickness decreases to a certain value, say 60 Å, the transition layer model becomes a significant factor in determining the values of N and T. In the table it is also seen that the abrupt model gives the least fitting error. These results, as well as the results for the thinner oxides of later sections, suggest that the interface of the Si-SiO_2 system is rather abrupt.

A group of the theoretically computed Δ, ψ curves *vs.* the incident angle in a wider range of 60-90° are shown in Fig. 3a and b, respectively. The curves are computed by employing the abrupt model for the oxide of 20, 40, 60, 80, and 100 Å, respectively. From these figures, it can be seen that the ψ data are much less sensitive to the thickness for the incident angle as compared to the Δ data. Also, for the Δ data, in order to obtain the highest sensitivity, it is desirable to measure the sample with the incident angle in the ranges of approximately 65-73° and/or of 77-83°. In Fig. 4a and b, the $d\Delta/dT$ and $d\psi/dT$ curves, which denote the sensitivities of Δ and ψ with respect to the oxide film in the

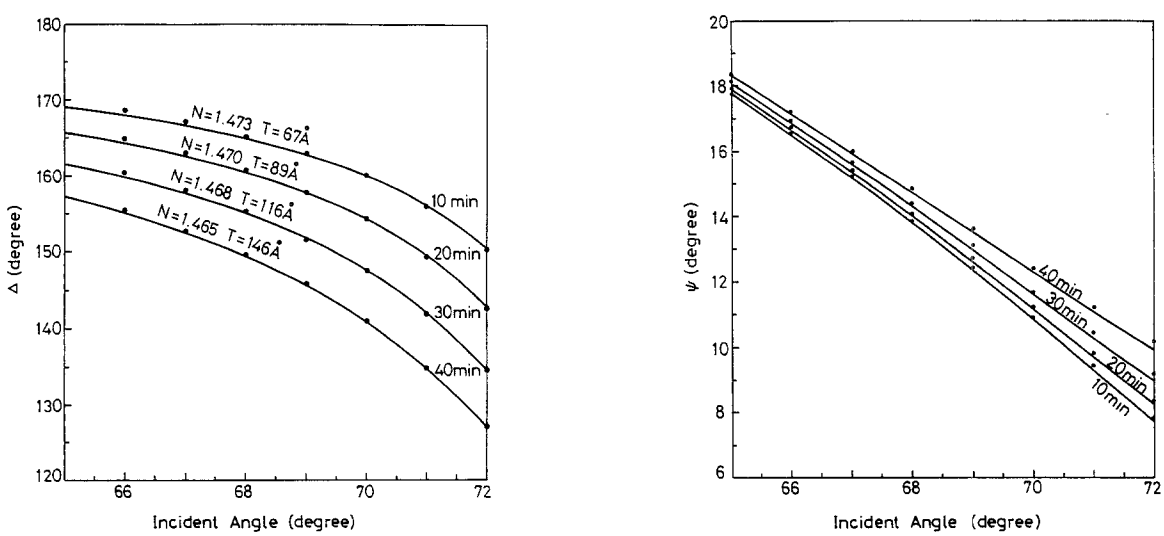

Fig. 2. (a, left) The measured data (dotted points) and the least squares error fitted curves (solid lines) of Δ for the SiO_2 oxidized in dry O_2 at 900°C for 10, 20, 30, and 40 min, respectively. (b, right) The measured data (dotted points) and the least squares error fitted curves (solid lines) of ψ for the SiO_2 oxidized in dry O_2 at 900°C for 10, 20, 30, and 40 min, respectively.

Table I. The refractive index (N), thickness (T), and the least squares error for ultrathin oxide films oxidized at 900°C for 10-40 min under different models.

Model	40′			30′			20′			10′		
	N	T	E_{rror}	N	T	E_{rror}	N	T	E_{rror}	N	T	E_{rror}
Abrupt	1 · 465	146	0 · 328	1 · 468	116	0 · 482	1 · 470	89	0 · 721	1 · 473	67	1 · 229
Exp/ox	1 · 466	145	0 · 597	1 · 466	116	1 · 198	1 · 468	89	1 · 487	1 · 473	67	1 · 548
Linear	1 · 464	147	0 · 601	1 · 464	117	1 · 195	1 · 466	91	1 · 481	1 · 470	69	1 · 544
Exp/sub	1 · 462	151	0 · 599	1 · 462	122	1 · 195	1 · 462	95	1 · 481	1 · 465	73	1 · 541

thickness range of 20-100 Å, respectively, are plotted. These figures reveal more clearly the above results, where $d\Delta/dT$ curves and $d\psi/dT$ curves differ more than one order in magnitude. Hence, for the MAI ellipsometry to measure the ultrathin oxide in the Si-SiO_2 system, only the $\Delta - \phi$ curve, where ϕ is the incident angle, needs consideration for its high sensitivity, and the incident angle should be in the range of 65-73° and/or 77-83°.

It is interesting to do error analysis on N and T with respect to the small variation of Δ, ψ, and ϕ. The errors of our system for Δ, ψ, and ϕ are 0.02°, 0.01°, and 0.01°, respectively. Figures 5a and b show theoretical plots for errors of N and T in percentage resulted from the deviations in Δ, ψ, and ϕ, respectively. In these figures, it is seen that errors increase with decrease of the thickness of the oxide; $d\psi$ causes the most significant errors and $d\phi$ causes negligible errors. Hence, if $\Delta - \phi$ data in the range of 65-73° are used to derive the values for N and T, the error is less than 1%.

Applications of MAI Ellipsometry

Measurement of native oxides.—It is known that a layer of native oxide of the thickness of 3-10 Å, depending on the processing conditions of the wafer, exists on the surface of Si wafers (28). Because this layer of native oxide is too thin, it is difficult to accurately measure its thickness and refractive index. This MAI ellipsometry is first applied to measure this native oxide layer. The samples were prepared by first cleaning the N-type (100), 4-5 Ω-cm, silicon wafers with the RCA cleaning process and dipped in the buffered HF solution and dried by N_2 (sample A). Part of the wafers were then oxidized in a hot H_2SO_4 solution for 10 min (sample B) and immediately measured by the MAI ellipsometer. After that both wafers (samples A and B) were placed at the exit of the tube of an oxidation furnace in an N_2 ambient at 900°C for 10 min, and the wafers were measured by MAI ellipsometer again. This was done because during the conventional oxidation process, the wafer to be oxidized was usually placed at the exit of the oxidation furnace in a flashing N_2 stream, waiting to be pushed into the furnace. It was to measure how thick the oxide was grown during this process. During this process, the samples A were denominated as sample C and samples B were denominated as samples D. Figure 6 shows the measured Δ for these samples in different incident angles. The corresponding fitted values for the thicknesses, refractive indexes, and the sum of the least squares fitting errors for these samples are shown in the insert. For these fittings, the abrupt model was used since it gave the least fitting error. From these data, it is seen that the samples dipped in the HF solution had the thinnest native oxide, and the thickness of this native oxide was approximately two to three atomic layers. It is known that boiling Si wafers in a hot H_2SO_4 solution gives a chemical oxide to wafers, and these oxides affect device characteristics significantly for the poly-emitter n^+-p diodes made on these wafers (29, 30). For B samples, the thickness of this chemical oxide measured by the MAI ellipsometry was 12 Å which was larger than the native oxide by another two atomic layers. These data verify that boiling a Si wafer in a hot H_2SO_4 solution does grow a chemical oxide on the wafer. For samples C and D, the thicknesses measured were 22 and 25 Å, respectively. Hence, exposing wafers at the exit of an oxidation furnace at a high temperature even in an N_2 ambient increases the thickness of the oxide. This indicates that carefulness should be exercised to grow the oxide of a thickness less than 50 Å since over 20 Å has already been grown before the wafer is pushed into the oxidation furnace. Finally, it is noted that the refractive indexes for all these samples are larger than 1.46 of the thick thermal oxide.

Measurement of the refractive indexes of ultrathin oxides.—As has been mentioned previously the value of the refractive index is one of the most important factors in determining the thickness of thin oxide by using the conventional ellipsometry. It has been reported (15, 16) that the thinner oxide has a higher refractive index. For example, Carim and Sinclair (4) suggested that a value as high as 1.7 could be used to compensate for the error in determining the oxide thickness. In this section, the refractive indexes of ultrathin thermal oxides, oxidized at different temperatures in the thickness range of 25-400 Å are measured by the MAI ellipsometry.

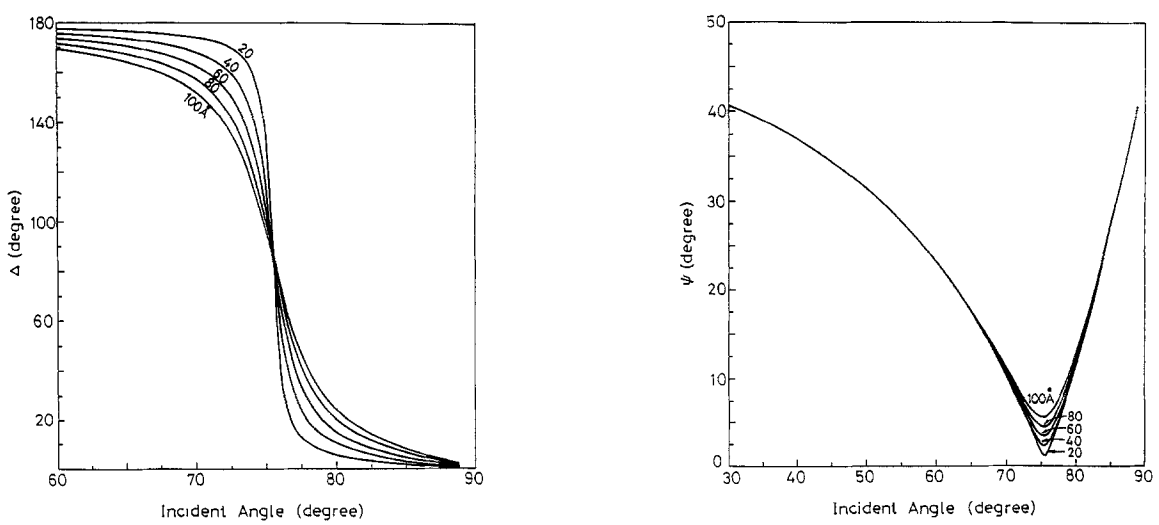

Fig. 3. (a, left) Simulated Δ curves with respect to the incident angle for various oxide thicknesses from 20 to 100 Å. (b, right) Simulated ψ curves with respect to the incident angle for various oxide thicknesses from 20 to 100 Å.

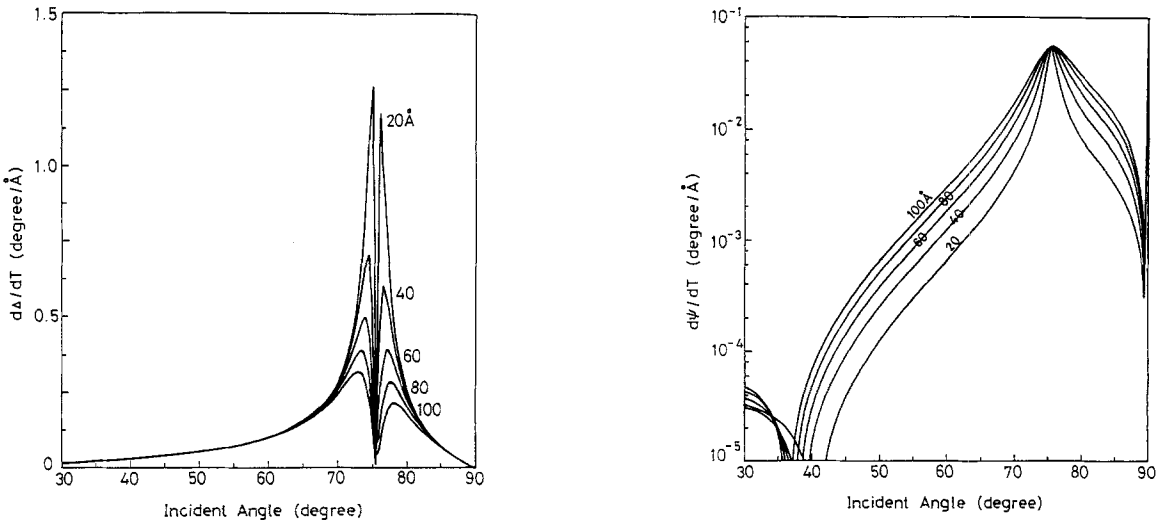

Fig. 4. (a, left) The sensitivity of Δ with respect to the thin-film thickness in different incident angles for various oxide thicknesses from 20 to 100 Å. (b, right) The sensitivity of ψ with respect to the thin film thickness in different incident angles for various oxide thicknesses from 20 to 100 Å.

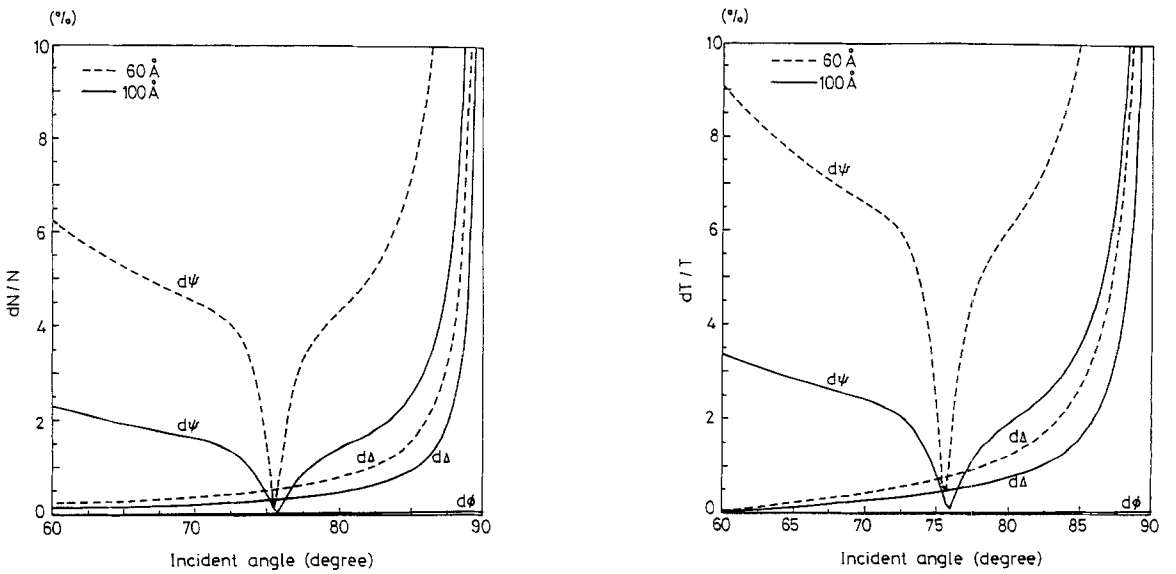

Fig. 5. (a, left) Errors of *N* due to the 0.02 deviation in Δ, 0.01 in ψ, and 0.01 in φ for a 60 and 100 Å oxide in different incident angles. (b, right) Errors of *T* due to the 0.02 deviation in Δ, 0.01 in ψ, and 0.01 in φ for a 60 and 100 Å oxide in different incident angles.

The samples were prepared by RCA cleaning the n-type (100), 4-5 Ω-cm, silicon wafers. The wafers were then dipped in the buffered HF solution and rinsed by DI water. They were pulled into the furnace in an N_2 ambient and oxidized in 1 atm dry O_2 at 800-1000°C for 10-40 min. The samples were measured by the MAI ellipsometer in the incident angles from 65 to 72°. As was done previously, the Δ − φ data were curve fitted to obtain the refractive indexes and the thicknesses by using the abrupt model. Figure 7 shows the measured refractive indexes with respect to the thickness for the various oxidation temperatures. It is seen that thinner oxides have higher refractive indexes, especially for oxides thinner than 100 Å. As the oxide thickness exceeds 200 Å, the refractive index approaches the value 1.46, of the bulk oxide. For oxides less than 100 Å, the refractive index increases rapidly with the decrease of the thickness. Also, from these data, it seems that the oxides grown at the high temperature have a higher refractive index.

Thermal growth kinetics of SiO_2 at the initial phase.—As early as 1966, Deal and Grove (31) proposed a space-charge effect model to explain the oxidation mechanism. The model successfully explains the oxidation kinetics in dry oxygen for the oxide thickness exceeding 350 Å. However, as the oxide is thinner than 350 Å, the model fails to explain the anomalous initial rapid oxidation phenomenon. Much study (32-35) has been done and various models have been proposed to explain and describe this phenomenon.

An accurate growth model of silicon oxidation is based on an accurate measurement of the thickness of oxide film. Since the MAI ellipsometry developed in this work can independently measure the accurate refractive index and thickness of the ultrathin oxide, the thicknesses of the ultrathin oxides of the previous section were also measured. The results of dry O_2 oxidation at 1 atm are plotted in Fig. 8 with respect to the growth time for several oxidation temperatures. It can be seen that all the growth curves, except the 1000°C one, are linear. For the 1000°C curve, there is an initial rapid growth region observed, and for the growth time larger than 10 min, the growth curve is also linear. The growth rate deduced from the curves for different oxidation temperatures are shown in the insert. The activation energy derived for these linear rate constants at different temperatures is 1.69 eV, which is somewhat different from the value of 1.76 eV obtained by other workers (6). In the figure, it is seen that all the curves cross at a point at the time axis of approximate minus 8 min. An empirical formula can be deduced from these curves as

$$d = y_o + A(t_{ox} + 8)$$

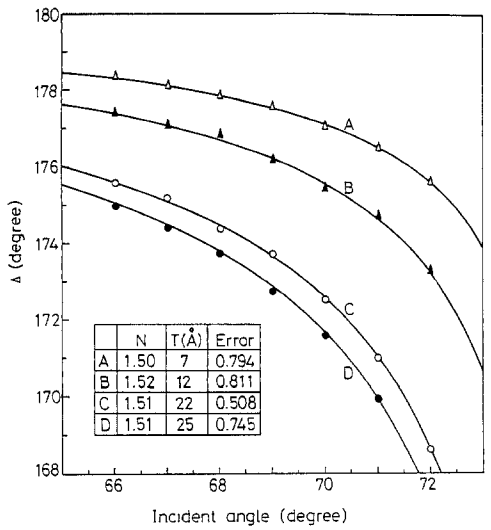

Fig. 6. The measured $\Delta - \phi$ data for the native oxides of Si wafers after different cleaning processes were applied. A is the sample right after RCA process and HF dipped, B is sample A oxidized in a hot H_2SO_4 solution for 10 min. C is sample A exposed at the exit of an oxidation furnace in an N_2 ambient at 900°C for 10 min, and D is sample B which exposed at the exit of an oxidation furnace in an N_2 ambient at 900°C for 10 min. Insert shows the fitted thicknesses and refractive indexes for these samples.

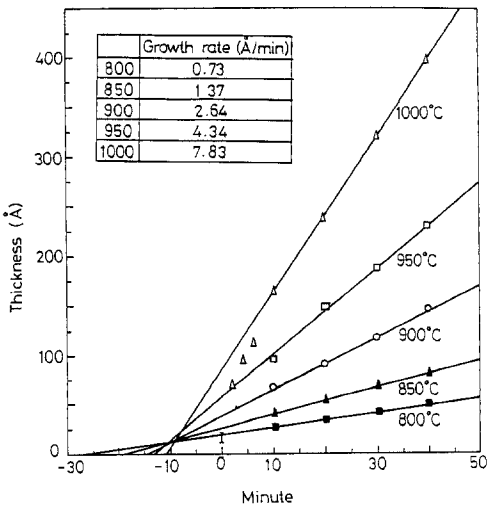

Fig. 8. The thickness with respect to the growth time for several oxidation temperatures. Insert shows the growth rate for each oxidizing temperature. The I at $t = 0$ indicates the measured thickness, 16-20 Å, of native oxide of silicon substrate.

where d is the thickness of oxide, y_0 is an effective native oxide thickness, A is the growth rate in Å/min at various temperatures, and t_{ox} is the oxidation time of the dry O_2. This empirical formula seems to say that for dry O_2 oxidation of ultrathin SiO_2, especially for an oxidation temperature below 950°C, the growth starts with an effective native oxide of 16-20 Å and grows linearly with respect to time, and it takes 8 min for the furnace to reach the steady oxidation state. This empirical formula will be useful for the computer process simulation such as SUPREM (36). In the figure, there are several data points at the $t = 0$ axis. These are the thicknesses for the oxides grown by inserting the wafers into the oxidation furnace without turning on O_2 but keeping N_2 flowing. These thicknesses are in the range of 16-20 Å. From these data points, it is seen that for an oxidation time less than 10 min, there exists the initial rapid oxidation phase (37). However, this initial rapid oxidation phase becomes insignificant as the oxidation temperature is below 850°C.

Conclusion

In this paper, the application of multiple-angle incident ellipsometry to measure the ultrathin oxide has been studied. The interfacial transition layer model, which affects the result of the measurement, has been investigated, and it has been found that the abrupt interfacial model is the most appropriate model for the SiO_2-Si interface. Sensitivity analyses done on the incident angle and the ellipsometry parameter error suggest that the MAI ellipsometry should be performed at the incident angle of 65-73° and/or 77-83°. The real application of this MAI ellipsometry to measure native oxides of silicon wafers has demonstrated the effectiveness of this ellipsometry. Also, by using this MAI ellipsometry, the native oxides of silicon wafers were found to be approximately two to three atomic layers after the wafers were buffered-HF etched and grown by another 15 Å after the wafers exposed at the exit of furnace in an N_2 ambient at high temperature. The refractive index of the ultrathin thermal oxide, measured by this MAI ellipsometry, has also been found to increase rapidly when the thickness of the oxide decreases below 100 Å. A simple empirical equation of oxidation in the linear region was obtained in this work. It is believed that these results are the most accurately measured results on the ultrathin oxides.

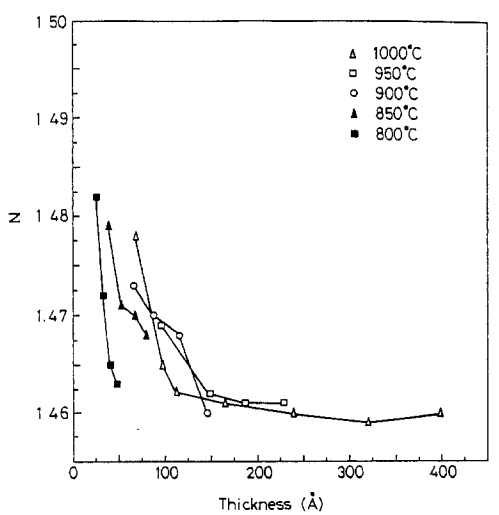

Fig. 7. The refractive indexes with respect to the thickness of ultrathin thermal oxides oxidized at various oxidation temperatures.

Manuscript submitted Sept. 4, 1990; revised manuscript received Jan. 16, 1991.

National Chiao Tung University assisted in meeting the publication costs of this article.

REFERENCES

1. S. M. Sze, "High Speed Semiconductor Devices," Wiley, New York (1990).
2. T. J. Coutts, "Active and Passive Thin Film Devices," Academic Press, Inc., New York (1978).
3. D. A. Baglee and P. L. Shah, "VLSI Electronics," Vol. 7, Chap. 4, Academic Press, Inc., New York (1985).
4. A. H. Carim and R. Sinclair, *This Journal*, **137,** 279 (1990).
5. Y. J. Van der Meuler, *ibid.*, **119,** 530 (1972).
6. H. Z. Massound, T. D. Plummer, and E. A. Irene, *ibid.*, **132,** 1754 (1985).
7. C. W. Jen, C. L. Lee, and T. F. Lei, *Solid State Electron.*, **27,** 1 (1984).
8. J. S. Witters, G. Groeseneken, and H. E. Maes, *IEEE Trans. Electron Devices,* **ED-36,** 1663 (1989).
9. R. M. A. Azzam and N. M. Bashara, "Ellipsometry and Polarized Light," North Holland Pub. Co., Amsterdam (1977).
10. R. J. Archer, *This Journal,* **104,** 619 (1957).
11. J. H. Ho, C. L. Lee, C. W. Jen, and T. F. Lei, *Solid-State Electron.*, **30,** 973 (1987).
12. J. H. Ho, C. L. Lee, and T. F. Lei, *ibid.*, **31,** 1321 (1988).
13. J. H. Ho, C. L. Lee, and T. F. Lei, *IEEE Trans. Instrum. Measure.*, Aug. (1990).

14. E. H. Nicollian and J. R. Brews, "MOS Physics and Technology," Wiley, New York (1982).
15. E. Taft and L. Cordes, *This Journal*, **126,** 131 (1979).
16. A. Kalnitsky, S. P. Tay, J. P. Ellul, S. Chongsawangvirod, J. W. Andrews, and E. A. Irene, *ibid.*, **137,** 234 (1990).
17. T. Hattori and T. Suzuki, *Appl. Phys. Lett.*, **43,** 470 (1983).
18. J. F. Wager and C. W. Wilmsen, *J. Appl. Phys.*, **50,** 874 (1979).
19. R. Flitch and S. I. Raider, *J. Vac. Science. Technol.*, **12,** 305 (1975).
20. J. Blane, C. J. Buiocchi, M. S. Abrahams, and W. E. Ham, *Appl. Phys. Lett.*, **30,** 120 (1977).
21. F. J. Grunthaner and J. Maser, "The Physics of SiO_2 and Its Interface," Proceedings of the International Topical Conference, p. 389, Pergamon Press, New York (1978).
22. O. L. Krivanek and J. H. Mazur, *Appl. Phys. Lett.*, **37,** 392 (1980).
23. I. W. Boyd and J. I. B. Wilson, *J. Appl. Phys.*, **62,** 3195 (1987).
24. G. E. Jellison and F. A. Modine, *J. Opt. Soc. Am.*, **72,** 1253 (1982).
25. P. G. Snyder, M. C. Rost, G. H. Bu-Abbud, and J. A. Woollam, *J. Appl. Phys.*, **60,** 3292 (1986).
26. F. L. McCrackin and J. P. Colson, "Ellipsometry in the Measurement of Surface and Thin Films," p. 61, Misc. Publ., Washington, DC (1964).
27. M. M. Ibrahim and N. M. Bashara, *J. Opt. Soc. Am.*, **61,** 1622 (1971).
28. M. C. Stork, M. Arienzo, and C. Y. Wong, *IEEE Trans. Electron Devices*, **ED-32,** 1766 (1985).
29. S. L. Wu, C. L. Lee, and T. F. Lei, *Appl. Phys. Lett.*, **56,** 1031 (1990).
30. P. Ashburn and B. Soerowirgjo, *IEEE Trans. Electron Devices*, **ED-31,** 853 (1984).
31. B. E. Deal and A. S. Grove, *J. Appl. Phys.*, **36,** 3770 (1966).
32. K. H. Yang, *This Journal*, **132,** 1214 (1985).
33. M. A. Hopper, R. A. Clarke, and L. Young, *ibid.*, **122,** 1216 (1975).
34. A. C. Adams, T. F. Smith, and C. C. Chang, *ibid.*, **127,** 1787 (1980).
35. V. Murali and S. P. Murarka, *J. Appl. Phys.*, **60,** 2106 (1986).
36. S. Wolf, "Silicon Processing for the VLSI ERA," Vol. 2, Chap. 9, Lattice Press, CA (1990).
37. H. Z. Massoud, J. D. Plummer, and E. A. Irene, *This Journal*, **132,** 2685 (1985).

A Composite Layer of Al-Er-O Particles in a Silicon Matrix

M. Salvi, H. L'haridon, P. N. Favennec, D. Moutonnet, M. Gauneau, and M. Kechouane[1]

CNET LAB/OCM BP 40 Route de Trégastel, 22301 Lannion, France

ABSTRACT

Erbium is of particular interest in telecommunication systems because of its sharp and intense photoemission at 1.54 μm. However, erbium is difficult to incorporate at high concentrations in the semiconductor matrix and presents a tendency to segregate in the material. A better solution would be to use the erbium impurity as an element of the matrix rather than as a dopant. Such a structure can be obtained with a garnet-like layer realized on a semiconductor substrate. Evaporation, implantation, and annealing techniques were combined to obtain a new ternary material Al-Er-O. These garnet-like layers were developed on silicon. The layer composition as well as the interaction of the different elements with the substrate were studied by Rutherford backscattering, secondary ion mass spectroscopy, and X analyses. The surface aspect variations were observed by scanning electron microscopy. According to the annealing conditions, a photoluminescence at about 1.54 μm corresponding to erbium emission was observed at 77 K. This luminescence is due to insulating microparticles composed of aluminum, erbium, oxygen, and possibly silicon.

In the past few years, erbium doping of III-V compound semiconductors and also of silicon was extensively studied (1-3). The intra 4-f shell transition of erbium leading to a sharp and intense photoemission at 1.54 μm is of great interest for telecommunications systems because this wavelength corresponds to the minimum absorption of silica-based optical fibers. Recent work on MBE epitaxy (4, 5) or on ion implantation (6, 7) showed the difficulty in incorporating high concentrations of erbium in the semiconductor matrix. In addition, we observed the creation of microparticles composed of erbium and oxygen by ion implantation in a semiconductor matrix (8). A cathodoluminescence study showed that the 1.54 μm emission is due only to these microparticles. However, the luminescence intensity is always limited by the experimental parameters. Consequently, we are trying to improve this emission intensity by introducing the erbium impurity as an element of the matrix, instead of a doping element. Such a structure can be obtained with a garnet-like layer realized on a semiconductor. In this paper, the realization of such a layer is presented. An aluminum layer pre-evaporated on a silicon substrate was subsequently implanted with very high doses of erbium and then annealed to obtain a new ternary material $Al_xEr_yO_z$.

Experimental

The silicon wafers used for this study are n-type, phosphorus doped, Czochralski-grown, <100>-oriented, provided by Wacker, Limited. The oxygen concentration in the bulk is about 10^{18} cm^{-3}. A 1000 Å thick aluminum layer is evaporated and then implanted with erbium ions (M = 166) with a dose of 2×10^{16} Er^+ cm^{-2}. In order to implant all the Al layer, a nearly flat profile is obtained by a dual implantation (130 and 330 keV). The annealings are performed under an oxidizing atmosphere, enabling oxygen

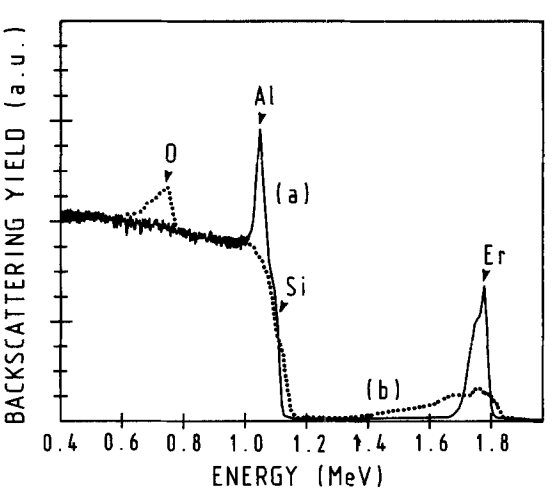

Fig. 1. RBS spectra: (a) ——— before annealing, (b) . . . . . after annealing (900°C, 1 h).

[1] Present address: Laboratoire "couches minces," USTHB, Institut de Physique, BP 32, El-Alia, Alger, Algeria.